HHS Public Access

Author manuscript

Matrix Biol. Author manuscript; available in PMC 2023 November 01.

Published in final edited form as:

Matrix Biol. 2022 November ; 113: 83–99. doi:10.1016/j.matbio.2022.10.001.

Optic neuropathy associated with TGFβ dysregulation in mice with a glaucoma-causative mutation of *Adamts10*

Hang-Jing Wu[1], **Rachel W. Kuchtey**[1,2], **John Kuchtey**[1,*]

[1]Vanderbilt Eye Institute, Vanderbilt University Medical Center, Nashville, TN, USA, 37232-8808

[2]Department of Molecular Physiology and Biophysics, Vanderbilt University, Nashville, TN, USA,37232-0022

Abstract

Glaucoma is a neurodegenerative disease that causes irreversible blindness due to loss of retinal ganglion cells (RGCs) and their axons. We previously identified a G661R mutation of *ADAMTS10* (A Disintegrin And Metalloproteinase with ThromboSpondin type 1 motif 10) as the disease-causing mutation in a beagle model of glaucoma. ADAMTS10 is a secreted matrix metalloproteinase that belongs to the ADAMTS family which is involved in extracellular matrix (ECM) turnover. Previous studies have shown that ADAMTS10 binds fibrillin microfibrils, promotes their formation, and influences their fibrillin isoform composition. Here, we established a mouse model carrying the G661R mutation of *Adamts10* (*Adamts10*$^{G661R/G661R}$) to investigate its ocular phenotypes related to glaucoma and to explore possible functions of ADAMTS10. We found that ADAMTS10 was expressed in the inner retina and along RGC axons in the optic nerve. However, ADAMTS10 was not colocalized with fibrillin microfibrils in these tissues, suggesting fibrillin-independent function for ADAMTS10. In electroretinogram experiments, we found that *Adamts10*$^{G661R/G661R}$ mice had reduced amplitude of retinal responses to dim light stimulus, indicating RGC dysfunction. The reduced RGC function coincided with RGC axon structural changes manifested as smaller optic nerves and fewer optic nerve axons, which may contribute to glaucoma. The reduced number of optic nerve axons found for *Adamts10*$^{G661R/G661R}$ mice occurred early, suggesting developmental deficits. Subsequent experiments found increased apoptosis in the retina of *Adamts10*$^{G661R/G661R}$ mice during postnatal development, which could result in fewer RGCs produced, accounting for fewer optic nerve axons in adulthood. Consistent with a protective effect of transforming growth factor β (TGFβ) signaling against apoptosis during retinal development as shown previously by others, we found increased apoptosis accompanied by decreased TGFβ signaling in the developing retina of *Adamts10*$^{G661R/G661R}$ mice, suggesting a novel role for ADAMTS10 in regulating TGFβ signaling which could involve direct interaction between ADAMTS10 and latent TGFβ.

*Corresponding Author: John Kuchtey, Vanderbilt Eye Institute, Vanderbilt University Medical Center, 1161 21st Ave S, AA7100 MCN, Nashville, TN 37232, john.kuchtey@vumc.org.

Declarations of interest: none.

Keywords

Glaucoma; Metalloprotease; Fibrillin microfibrils; Extracellular matrix; TGFβ signaling

Introduction

Glaucoma is a neurodegenerative disease that is the leading cause of irreversible vision loss which is specifically due to optic nerve axon degeneration and death of retinal ganglion cells (RGCs).[1,2] Risk factors for glaucoma include elevated intraocular pressure, advanced age, and family history of glaucoma. Previously, we identified a G661R variant in the cysteine-rich domain of *ADAMTS10* as disease-causative in a colony of beagles with autosomal recessive glaucoma.[3] ADAMTS10 belongs to the ADAMTS family of secreted matrix metalloproteinases that includes 19 ADAMTS and 7 ADAMTS-like (ADAMTSL) proteins.[4] ADAMTS proteinases are pivotal components of the ECM that are involved in ECM turnover. The finding that a mutation in *ADAMTS10* causes glaucoma has been validated by the discovery of another variant of *ADAMTS10*, A387T, as the glaucoma-causative variant in Norwegian Elkhounds.[5] Subsequent studies showed that mutations in *ADAMTS17* cause glaucoma in four other dog breeds [5–8] and mutations of *ADAMTS8* [9–11], *ADAMTS2* [12] and *ADAMTSL1* [13] are associated with glaucoma traits or cause glaucoma in humans, further supporting the causative effect of *ADAMTS* mutations in glaucoma.

Mutations in *ADAMTS10* also cause autosomal recessive Weill-Marchesani syndrome (WMS), a connective tissue disorder characterized by short stature and ocular phenotypes, including lens dislocations, in humans.[14–16] Mutations in *FBN1,* the gene encoding fibrillin-1, cause autosomal dominant WMS [17,18] which is indistinguishable from autosomal recessive WMS, suggesting that fibrillin1 and ADAMTS10 have overlapping function.[19,20] ADAMTS10 binds to fibrillin-1 with high affinity and is co-expressed with fibrillin-1 in human dermis and lens zonules.[21–23] ADAMTS10 can cleave fibrillin-1 or fibrillin-2 after optimizing its furin recognition site *in vitro* [21,24] and genetic manipulation of *Adamts10* in mice resulted in alteration of fibrillin isotype composition of microfibrils *in vivo*.[22–24]

In addition to WMS, mutations in *FBN1* cause Marfan syndrome (MFS),[25–27] a connective tissue disorder characterized by tall stature, the opposite systemic phenotype of WMS, but with lens dislocation similar to WMS. Microfibrils composed of fibrillin-1 and fibrillin-2 bind to latent transforming growth factor β (TGFβ) binding protein and regulate TGFβ and bone morphogenic protein (BMP) signaling.[28] In the canonical signaling pathway, TGFβ superfamily members signal through transmembrane serine/threonine kinase receptors to activate intracellular Smad proteins by phosphorylation. Phosphorylated Smad (pSmad) translocates into the nucleus to regulate gene transcription, playing key roles throughout development and in adult homeostatic processes.[29] Dysregulated TGFβ signaling has been proposed to be involved in the pathogenesis of MFS and WMS [18,30–32] and has long been implicated in the pathogenesis of glaucoma.[33]

We recently reported that mice carrying the same G661R variant of *Adamts10* (*Adamts10*$^{G661R/G661R}$) as found in beagles with glaucoma, recapitulated features of WMS and showed alteration of fibrillin isoform composition of ocular microfibrils.[23] Unlike in the dogs, intraocular pressure was not changed in *Adamts10*$^{G661R/G661R}$ mice.[23] In the current study, we investigated whether *Adamts10*$^{G661R/G661R}$ mice developed glaucoma phenotypes in the optic nerve and retina and explored potential underlying mechanisms.

Results

ADAMTS10 expression in the retina and optic nerve

Relevant structures of the eye are shown in schematic diagrams with zoom in views of the retina and optic nerve (Fig. 1A). RGC cell bodies are located in the inner most cellular layer of the retina, the ganglion cell layer (GCL). RGC axons form the retinal nerve fiber layer (RNFL) and project to the brain through the optic nerve.

ADAMTS10 expression was examined in the retina and optic nerve by immunofluorescent staining using an antibody that we used previously and showed detection of a single band at the expected MW in Western blots of lysates from cells transfected with an ADAMTS10 expression vector.[3] In the retina, the highest intensity ADAMTS10 immunofluorescence was found in the RNFL (white dashed box, Fig. 1B) which is mainly composed of RGC axons. ADAMTS10 immunofluorescence was also found in the inner plexiform layer (IPL, Fig 1B, E and E') which is partly composed of RGC dendrites. In the optic nerve, ADAMTS10 immunofluorescence was found running parallel with the optic nerve axons (Fig. 1B, E and E'). Co-staining with a marker specific for RGCs in the retina (βIII tubulin, Fig. 1C) showed extensive overlap with ADAMTS10 in the RNFL and in the optic nerve (Fig. 1 E and E') indicating localization of ADAMTS10 with RGC axons. High magnification images from co-staining for ADAMTS10 (Fig. 1F) with an RGC cytoplasmic marker, RBPMS (Fig. 1G) showed that ADAMTS10 immunofluorescence was associated with RGC cell bodies (Fig. 1I, arrowheads). In optic nerve cross-sections, co-staining for ADAMTS10, βIII tubulin and the glial cell marker GFAP confirmed colocalization of ADAMTS10 with optic nerve axons but showed no overlap of ADAMTS10 with glial cells (Fig. 1 J - O). DAPI staining is shown (Fig. 1D, H and L). Comparisons between wt and *Adamts10*$^{G661R/G661R}$ mice showed no prominent differences in the distribution pattern or immunofluorescence intensity of ADAMTS10 in the retina and optic nerve, though an age-dependent enhancement of ADAMTS10 immunofluorescence was observed in the optic nerve (Supplementary Figure).

Wt and G661R mutant forms of human ADAMTS10 are secreted

To investigate whether the wt and G661R mutant forms of ADAMTS10 are secreted, HEK293T cells were transfected with expression vectors encoding either wt or G661R mutant forms of FLAG-tagged human ADAMTS10. 72h post-transfection, supernatants and cell lysates were collected for Western blotting using an anti-FLAG antibody. Single bands at the expected MW of approximately 130 kDa were detected in supernatants as well as lysates from cells that were transfected with either wt or G661R mutant forms of human ADAMTS10, but not in cells that were mock transfected without vectors (Fig. 2A). Band

intensities were similar for cells transfected with either wt or G661R mutant constructs, suggesting that the G661R mutation does not affect secretion of ADAMTS10. To further confirm that the wt and G661R mutant forms of ADAMTS10 are secreted, anti-FLAG immunocytochemistry was performed on intact non-permeabilized HEK293T cells that were transfected with FLAG-tagged human ADAMTS10 constructs. Anti-FLAG fluorescent signals were similar in cultures of non-permeabilized cells that were transfected with wt or G661R mutant forms of FLAG tagged human ADAMTS10 plasmids (Fig. 2B), suggesting that the G661R mutation does not interfere with ADAMTS10 secretion. Fluorescent signals were not detected from cells that were transfected without vectors (Fig. 2B).

ADAMTS10 expression independent of microfibrils in the retina and optic nerve

Genetic evidence suggests functional interaction between ADAMTS10 and fibrillin-1 and ADAMTS10 has been shown to colocalize with fibrillin microfibrils in human skin and lens zonules.[21,22] To investigate colocalization of ADAMTS10 with fibrillin-1, sagittal sections of eyes from wt and *Adamts10*$^{G661R/G661R}$ mice at 3 months of age were immunostained with antibodies to ADAMTS10 (Fig. 3A and E) and fibrillin-1 (Fig. 3B and F). Fibrillin-1 immunofluorescence was detected in the optic nerve meninges, including the pia mater and dura mater (Fig. 3B and F) while ADAMTS10 was restricted to the optic nerve (Fig. 3A and E). Like the optic nerve, the inner retina was positive for ADAMTS10 immunofluorescence but negative for fibrillin-1 immunofluorescence (Fig. 3A, E and B, F). This expression pattern resulted in an apparent total lack of overlap between fibrillin-1 and ADAMTS10 (Fig. 3D and H). To determine if the lack of detectable fibrillin-1 in the optic nerve and retina was due to lack of microfibrils, sections were immunostained for a general marker for microfibrils, microfibril-associated glycoprotein 1 (MAGP1).[34] MAGP1 immunofluorescence fully overlapped with fibrillin-1 immunofluorescence in the pia mater and dura mater (Fig. 3L and P) but was not detectable in the retina or optic nerve (Fig. 3I, M and J, N), suggesting lack of microfibrils in these structures. Lack of colocalization of ADAMTS10 with microfibrils suggests a role for ADAMTS10 that is independent of fibrillin microfibrils. Note that the immunofluorescence intensities and expression patterns of ADAMTS10, fibrillin-1 and MAGP1 were comparable between wt and *Adamts10*$^{G661R/G661R}$ mice (Fig. 3), suggesting that ADAMTS10 expression and formation of fibrillin microfibrils in the retina and optic nerve are not affected by the G661R mutation of Adamts10.

Reduced inner retinal function in *Adamts10*$^{G661R/G661R}$ mice

To determine if *Adamts10*$^{G661R/G661R}$ mice have reduced RGC function indicative of glaucoma, scotopic (dark-adapted) electroretinogram (ERG, a method to measure the electrical activity of the retina in response to light stimuli) was performed on mice at 3–5 months of age. ERG waveforms were elicited by a series of flash stimuli. At a low stimulus intensity of −4 log cd·s/m^2, waveforms displayed well-defined positive scotopic threshold responses (pSTR; Fig. 4A, green arrowhead), which is mainly driven by RGCs.[35–38] With increasing stimulus intensities, waveforms became dominated by outer retinal responses consisting of photoreceptor-driven a-waves rapidly followed by bipolar cell-driven b-waves (Fig. 4A, red and blue arrowheads).

Amplitudes and latencies (time intervals between stimulus onset and peak/trough of response) were analyzed at a stimulus intensity of −4 log cd·s/m^2 for pSTR and at 0 log cd·s/m^2 for a- and b-wave responses. Significantly reduced pSTR amplitude was found for *Adamts10*$^{G661R/G661R}$ mice, compared with wt (74.9 ± 14.6 *vs.* 89.6 ± 20.4 μV, p = 0.03, Fig. 4B) likely indicating lower RGC responses. The reduction in RGC responses could be due to reduced input from bipolar cells. However, Amplitudes of a- and b-wave responses were not statistically different between wt and *Adamts10*$^{G661R/G661R}$ mice (Fig. 4C and D) indicating that the reduced pSTR amplitude is not due to a reduction of bipolar cell responses. Latencies for each response were not statistically different (Fig. 4E - G).

Optic nerve analysis

To determine whether there is any optic nerve pathology in *Adamts10*$^{G661R/G661R}$ mice, epon-embedded optic nerves from mice at 3, 6, and 24 months of age were cross sectioned, stained with p-phenylenediamine (PPD) and examined by high-resolution light microscopy. Optic nerves from *Adamts10*$^{G661R/G661R}$ mice appeared to be smaller than wt (Fig. 5A). For all three time-points, the mean optic nerve area of *Adamts10*$^{G661R/G661R}$ mice was significantly smaller than wt (Fig. 5B): 8.6% smaller at 3 months (p = 0.003), 12.6% smaller at 6 months (p = 0.002) and 13.5% smaller at 24 months (p < 0.0001). A significant age-dependent expansion of the optic nerve was found (Fig. 5B) that was similar for wt and *Adamts10*$^{G661R/G661R}$ mice, with a 50.6% increase for *Adamts10*$^{G661R/G661R}$ and a 59.0% increase for wt from 3 to 24 months of age (both p < 0.0001). The increase of optic nerve size with increased age is consistent with our previous data [39] and other works [40,41].

Since loss of optic nerve axons due to death of retinal ganglion cells is a defining feature of glaucoma, the number of axons in optic nerves of wt and *Adamts10*$^{G661R/G661R}$ mice was determined. A reduction in the number of optic nerve axons was observed in *Adamts10*$^{G661R/G661R}$ mice compared to wt (Fig. 5C), with 6.9% fewer at 3 months (p = 0.01), 17.5% fewer at 6 months (p = 0.0003) and 9.4% fewer at 24 months (p = 0.01).

Although a trend towards smaller axons was observed in *Adamts10*$^{G661R/G661R}$, median axon diameter was not significantly different between wt and *Adamts10*$^{G661R/G661R}$ mice at 3, 6 and 24 months of age (Fig. 5D). The median axon diameter increased with age for both wt and *Adamts10*$^{G661R/G661R}$ mice (all p < 0.009), consistent with our previous results.[39]

Increased apoptosis and decreased pSmad2 signaling in the retinas of *Adamts10*$^{G661R/G661R}$ mice

The reduction in the number of RGC axons for *Adamts10*$^{G661R/G661R}$ mice occurred early, suggesting that fewer RGCs were produced during retinal development. The final number of retinal neurons is partially determined by the number of cells undergoing apoptosis. Apoptotic cells in the retina of wt and *Adamts10*$^{G661R/G661R}$ mice were detected using TUNEL assay at postnatal day 10 (P10). At P10, TUNEL-positive apoptotic nuclei primarily localized in the inner nuclear layer (INL) and GCL of the retina and appeared to be more numerous for *Adamts10*$^{G661R/G661R}$ mice compared to wt (Fig. 6A). Quantitative analysis by counting TUNEL-positive nuclei in the GCL revealed a 37.2% increase in the number of apoptotic cells for *Adamts10*$^{G661R/G661R}$ mice compared to wt (Fig. 6B, 4.06 ± 1.25 *vs.* 2.96

± 1.36, mean ± SD, p = 0.03). Increased apoptosis in the GCL would decrease the number of RGCs surviving development and reduce the number of RGC axons in the optic nerve of *Adamts10*$^{G661R/G661R}$ mice.

Since it has been shown that TGFβ signaling protects retinal neurons from apoptosis during eye development,[42] we next examined TGFβ signaling in the retina of wt and *Adamts10*$^{G661R/G661R}$ mice by immunofluorescent staining of pSmad2 on sagittal eye sections from mice at P10. Overall, fluorescent intensity of pSmad2 appeared to be lower for *Adamts10*$^{G661R/G661R}$ mice compared to wt (Fig. 6C). Occasionally, segments of retina with absent pSmad2 immunofluorescence but well-preserved nuclei were observed in *Adamts10*$^{G661R/G661R}$ mice (Fig. 6C, yellow arrowheads). Quantitative analysis showed that the mean fluorescent intensity of pSmad2 was significantly lower in the GCL for *Adamts10*$^{G661R/G661R}$ mice compared to wt (Fig. 6D) suggesting reduced TGFβ signaling which would result in reduced protection from apoptosis during retinal development.

ADAMTS10 forms interaction complex with TGFβ1

Previous work has shown that two other ADAMTS family members, ADAMTS1 and ADAMTS16, form complexes with and activate TGFβ by displacing its latency associated peptide (LAP) and exposing the active portion of TGFβ.[43,44] To determine if ADAMTS10 forms a complex with TGFβ, we performed proximity ligation assays with HEK293T cells co-transfected with a plasmid encoding either wt or G661R mutant forms of FLAG-tagged ADAMTS10 together with a plasmid encoding TGFβ1. Robust fluorescent signal, indicative of close (< 40 nm) interaction between ADAMTS10 and TGFβ1 was detected in cells co-transfected with TGFβ1 and wt or G661R mutant ADAMTS10 constructs (Fig. 7A and B). No signal was detected in the control group that omitted primary antibodies (Fig. 7C). These results suggest that regulation of TGFβ by ADAMTS10 could involve direct protein-protein interactions between LAP-TGFβ1 and ADAMTS10.

Discussion

In this study, we investigated the functions of ADAMTS10 and its association with a neurodegenerative disease. Using mice that carry the G661R mutation of *Adamts10* that is known to cause glaucoma in dogs,[3,23] we investigated the expression pattern of ADAMTS10 and the effects of the G661R mutation on neuronal function and optic nerve structure and explored the underlying mechanism. We found that ADAMTS10 is predominantly colocalized with RGC cell bodies and axons in the retina and in the optic nerve as shown by immunostaining for ADAMTS10 and β III tubulin or RBPMS (Fig. 1). This distinctive expression pattern is consistent with ADAMTS10 being a glaucoma-causative gene since degeneration of RGCs and their axons is the defining feature of glaucoma. Presumably since it is a secreted protein,[45] ADAMTS10 is localized to the extracellular space adjacent to axons.

We confirmed that the normal form of ADAMTS10 is secreted by Western blotting of cell supernatants and immunocytochemistry of non-permeabilized ADAMTS10-transfected cells (Fig. 2), similar to Somerville et al.[45] Since WMS-causing mutations that prevent normal secretion of ADAMTS10[16] and ADAMTS17[46] have been identified, we investigated

the secretory properties of G661R-mutated ADAMTS10. For cells transfected with G661R ADAMTS10, Western blotting of cell supernatants showed bands of the expected MW and of similar intensity to that from cells transfected with normal ADAMTS10 (Fig. 2A). In addition, immunocytochemistry of non-permeabilized cells was similar for cells transfected with normal or mutated forms of ADAMTS10, with staining patterns suggesting cell-associated and extracellular matrix expression (Fig. 2B). These findings indicate that the G661R mutation does not interfere with secretion of ADAMTS10.

In the optic nerve and retina of adult mice we found an apparent complete lack of colocalization of ADAMTS10 with microfibrils by co-immunostaining for ADAMTS10 and fibrillin-1 or MAGP1 (Fig. 3). ADAMTS10 immunostaining brightly labeled RGC axons in the retina and optic nerve while fibrillin-1 or MAGP1 immunofluorescence was below detection. In the pia mater and dura mater, which are adjacent to the optic nerve, bright fibrillin-1 and MAGP1 immunofluorescence was observed which is expected since these tissues are rich in elastic fibers and all elastic fibers are ensheathed in fibrillin microfibrils.[47] The lack of colocalization of ADAMTS10 with fibrillin microfibrils is somewhat unexpected since ADAMTS10 has previously been shown to bind fibrillin-1 with high affinity [18,21] and to colocalize with fibrillin-1 and microfibrils in the dermis [21] and as we and others have shown, in the lens zonules.[22,23] In addition, colocalization of ADAMTS10 with microfibrils would be expected for ADAMTS10 to fulfill its function to proteolyze fibrillin-1 and fibrillin-2 which have been identified as substrates of ADAMTS10.[21,24] In the retina and optic nerve, expression of ADAMTS10 in the apparent absence microfibrils suggests a function for ADAMTS10 that is independent of microfibrils. ADAMTS10 may have functions in addition to its metalloproteinase capability or if it is acting as a protease, it may have substrates in addition to fibrillins. Identifying unknown substrates for ADAMTS10 and relating them to disease processes such as glaucoma are intriguing subjects for further investigation.

Examination of retinal function by ERG showed that pSTR responses, which are primarily driven by RGCs,[35–38] are reduced in $Adamts10^{G661R/G661R}$ mice (Fig. 4). The amplitude of the pSTR is partly determined by the magnitude of signal input from bipolar cells to RGC dendrites. However, the bipolar cell responses, as determined by the b-wave amplitude, were not reduced in $Adamts10^{G661R/G661R}$ mice, indicating that the reduction in pSTR is not caused by reduced bipolar cell input. In the setting of normal b-waves, reduced pSTR amplitudes in $Adamts10^{G661R/G661R}$ mice indicate that the G661R mutation of *Adamts10* causes dysfunctional RGC responses. The intense ADAMTS10 immunofluorescence localized to RGC dendrites, cell bodies and axons is consistent with the observed functional deficits of RGCs in $Adamts10^{G661R/G661R}$ mice.

In addition to functional deficits of the retinal responses, the optic nerves of $Adamts10^{G661R/G661R}$ mice displayed structural abnormalities (Fig. 5). $Adamts10^{G661R/G661R}$ mice had small optic nerves with a trend towards smaller optic nerve axons, suggesting optic nerve pathology which may be relevant to glaucoma. Previously, we reported that mice with the *Tsk* mutation of *Fbn1* ($Fbn1^{Tsk/+}$) had larger optic nerves and larger optic nerve axons in the setting of normal intraocular pressure.[39] By experimentally inducing elevated intraocular pressure, we found that $Fbn1^{Tsk/+}$ mice are more susceptible

to optic nerve axon loss compared to wt.[48] These findings suggest that mice with abnormal optic nerve size are more vulnerable to pressure-induced glaucoma. The optic nerve pathology found in *Adamts10*$^{G661R/G661R}$ mice may result in increased susceptibility to glaucoma.

Mutations in *FBN1* and *ADAMTS10* both cause WMS in humans,[14,17,18] suggesting overlapping functions of fibrillin-1 and ADAMTS10. However, mutations in *FBN1* also cause MFS,[25–27] which has musculoskeletal phenotypes that are the opposite of WMS. As discussed above, our current finding of small optic nerves in *Adamts10*$^{G661R/G661R}$ mice is opposite to our previous finding of enlarged optic nerves in *Fbn1*$^{C1039G/+}$ (data not published) and *Fbn1*$^{Tsk/+}$ mice,[39] suggesting opposing effects of mutations in *Adamts10* and *Fbn1*. Similarly, we have found that *Fbn1*$^{C1039G/+}$ (data not published) and *Fbn1*$^{Tsk/+}$ mice have thin corneas [39] while *Adamts10*$^{G661R/G661R}$ mice have thick corneas.[23] We have also found that the anterior chamber depth is shallow in *Adamts10*$^{G661R/G661R}$ mice [23] while tissue-specific knockout of *Fbn1* has been shown to cause deeper anterior chambers,[49] further suggesting opposing effects of mutations in *Adamts10* and *Fbn1*. A similar relationship is found comparing MFS and WMS, with thin corneas and deep anterior chambers in MFS[50] and thick corneas and shallow anterior chambers found in WMS patients.[51] However, it should be noted that autosomal dominant WMS caused by mutations in *FBN1* cannot be distinguished from autosomal recessive WMS caused by mutations in *ADAMTS10*.[19]

The reduction in the number of optic nerve axons in *Adamts10*$^{G661R/G661R}$ mice was observed as early as 3 months of age (Fig. 5). One possible explanation for the reduced axon number is that fewer RGCs were produced during development. Braunger et al. have shown that TGFβ protects against apoptosis of retinal neurons which occurs primarily during the first 2 postnatal weeks.[42] They showed that mice with a TGFβ type II receptor deficiency had significantly increased apoptotic retinal neurons during embryonic and postnatal development, suggesting TGFβ signaling to be neuroprotective.[52] Using the zebrafish model system, we have recently found that injecting embryos with a morpholino designed to reduce expression of *adamts10* strongly inhibited TGFβ signaling in the developing eye.[53] Therefore, we hypothesized that the G661R mutation of *Adamts10* results in reduced TGFβ signaling and increased apoptosis in the developing GCL and consequently causes a reduction in the number of RGCs produced during development. In this study, by pSmad2 immunostaining, we found a reduction of TGFβ signaling in the GCL of the developing retina of *Adamts10*$^{G661R/G661R}$ mice compared to wt at P10 (Fig. 6). The reduced TGFβ signaling coincided with increased apoptosis in the GCL which would result in fewer RGCs surviving apoptosis (Fig. 6). This is consistent with our hypothesis that the reduced number of RGCs is in part a result of fewer RGCs produced during development due to reduced TGFβ signaling in *Adamts10*$^{G661R/G661R}$ mice. These findings suggest previously unknown functions of ADAMTS10 both as a regulator of TGFβ signaling and as a contributor to retinal development.

We observed prominent TGFβ family signaling in the ganglion cell layer of the retina where we did not detect microfibrils by staining for either fibrillin-1 or MAGP1 (Figs. 6 and 3). It is not clear how ADAMTS10 regulates TGFβ activation in the retina, but our

findings suggest that it cannot be mediated by fibrillin microfibrils. TGFβ is secreted and incorporated into the ECM as part of a large latency complex (LLC) which includes the active form of TGFβ, the latency associated peptide (LAP) which blocks exposure of active TGFβ, and latent TGFβ binding protein (LTBP).[54] The LLC binds to ECM components including fibrillin microfibrils .[54] Activation of TGFβ can occur through cleavage of LAP by MMP2/9 [55] and other proteases such as plasmin.[56] ADAMTS10 could directly mediate TGFβ activation by cleaving LAP.

Alternatively, ADAMTS10 could activate TGFβ similar to thrombospondin-1 (TSP1). [57–59] TSP1 has been shown to activate TGFβ by interacting with LAP-TGFβ through WxxW and KRFK amino acid motifs which is thought to induce a confirmational change in LAP, thereby exposing active TGFβ to its receptors.[58] Interestingly, ADAMTS1 and ADAMTS16, include WxxW motifs in their first thrombospondin repeat domains and motifs similar to KRFK in their cysteine-rich domains. ADAMTS1 and ADAMTS16 have been shown to interact through those domains and activate LAP-TGFβ, similar to TSP1.[43,44] Analysis of ADAMTS10 amino acid sequence reveals potential interaction motifs (WTPW and IPFR) in the first TSP1 and cysteine rich domains, similar to those found in ADAMTS1 and ADAMTS16, suggesting possible direct activation of TGFβ by ADAMTS10 through interactions with LAP-TGFβ. Our finding that ADAMTS10 and LAP-TGFβ form a complex as determined by proximity ligation assay of transfected cells (Fig. 7) suggests that the mechanism of activation of TGFβ by ADAMTS10 could be similar to the direct activation mediated by TSP1, ADAMTS1, and ADAMTS16. While the G661R mutation did not appear to grossly reduce ADAMTS10/LAP-TGFβ complex formation, it could affect subsequent steps required to expose the active form of TGFβ for interaction with TGFβ receptors.

In conclusion, we found that *Adamts10*$^{G661R/G661R}$ mice exhibit ocular pathology that may be relevant to glaucoma, including RGC dysfunction, smaller optic nerves and fewer optic nerve axons. These abnormalities may increase susceptibility of the optic nerve to degeneration in response to stress. The reduction in the number of optic nerve axons in *Adamts10*$^{G661R/G661R}$ mice may be due in part to reduced TGFβ signaling and consequently increased apoptosis in the GCL of the developing retina. The reduction of TGFβ signaling in *Adamts10*$^{G661R/G661R}$ mice suggests a previously unknown function of ADAMTS10 in regulating TGFβ signaling which may involve direct interaction between ADAMTS10 and LAP-TGFβ and is altered by the G661R mutation. The lack of colocalization of ADAMTS10 with fibrillin microfibrils in the retina and optic nerve found in this study indicates currently unknown functions of ADAMTS10 that are independent of fibrillins.

Experimental procedures

Animals

All animal studies were performed in accordance with the statement for the Use of Animals in Ophthalmic and Vision Research of the Association for Research in Vision and Ophthalmology and were approved by the Institutional Animal Care and Use Committee of Vanderbilt University. Mice carrying the G661R mutation of *Adamts10* were generated using CRISPR-Cas9, as described in our previous publication.[23] Mice heterozygous

for G661R mutation of *Adamts10* were bred to produce cohorts of experimental animals homozygous for the G661R mutation of *Adamts10*, hereafter referred to as *Adamts10*$^{G661R/G661R}$, and control animals homozygous for wild-type *Adamts10*, hereafter referred to as wt. The genotype of each mouse was determined at weaning and confirmed after sacrificing. Animals were housed in a facility operated by the Vanderbilt University Division of Animal Care, with 12/12 h light/dark cycle and *ad libidum* access to food and water.

Immunofluorescence staining

Mice were sacrificed by CO_2 inhalation then cardiac perfused with PBS followed by 4% PFA in PBS. Eyes were enucleated, embedded in paraffin then sectioned at 7 μm thickness. Central sagittal eye sections were deparaffinized, rehydrated and then subjected to antigen retrieval with 20 μg/ml Proteinase K (Macherey-Nagel, Germany) for 5 min at room temperature. Sections were blocked with 5% normal donkey serum for 2 hours at room temperature in a humid chamber, then incubated with primary antibody (Table. 1) overnight at 4 °C. Slides were washed then incubated with appropriate secondary antibody (Alexa Fluro 488 conjugated donkey anti-goat, Alexa Fluro 546 conjugated donkey anti-mouse or donkey anti-rabbit or Alexa Fluro 647 conjugated donkey anti-rabbit) diluted 1:1000 for 2 hours, protected from light. Slides were washed again and cover-slipped with mounting medium containing DAPI (Prolong Gold, Thermo Fisher Scientific). Images were acquired under identical settings using Olympus FV1000 confocal microscopy equipped with 20X 0.5 NA objective. Stacks of optical sections were visualized as maximum-intensity z-projection using ImageJ (https://imagej.nih.gov/ij/index.html).

For pSmad2 staining, antigen retrieval was performed by immersing slides in sodium citrate buffer (pH = 8) for 15 min at 95 °C. Images were acquired using an upright fluorescence microscope (Nikon, Japan) equipped with a 20× 0.75 NA objective and CMOS camera (Hamamatsu ORCA-Flash 4.0, Japan). Mean fluorescence intensity of pSmad2 was quantified in ImageJ. pSmad2 fluorescence in the GCL was determined by subtracting the background intensity within the adjacent IPL from the fluorescence intensity within a mask drawn around the GCL.[61] Negative control immunostaining omitting primary antibodies were performed for each experiment and showed no fluorescence.

Transfection and Western Blotting

HEK293T cells (CRL-3216, ATCC, Manassas, VA) were cultured at 37 °C in Dulbecco's Modified Eagle's Medium (DMEM) supplemented with 10% fetal bovine serum in a humidified incubator with 5% CO_2 atmosphere. Cells cultured in 6-well plates were transfected with wt (Cat. # RC215901, OriGene Technologies) or the G661R mutant form[3] of human ADAMTS10 plasmid using Lipofectamine 3000 (Thermo Fisher Scientific) following manufacturer's instructions. Cells transfected without plasmid served as control. 6 h after transfection, serum-containing DMEM was replaced with reduced-serum medium (Opti-MEM, Thermo Fisher Scientific) and cells cultured for an additional 48 – 72 h. Conditioned medium was collected in tubes with protease and phosphatase inhibitor cocktail (Cat.# 78442, Thermo Fisher Scientific) and centrifuged at 12,000 rpm for 10 min at 4 °C. Supernatants were transferred to an Amicon Ultrafiltration Unit (Millipore) with a 50 kDa

cut-off membrane and concentrated ~50-fold. Cells layers were lysed in RIPA buffer with protease and phosphatase Inhibitor cocktail, sonicated for 1 min on ice and centrifuged at 12,000 rpm for 10 min at 4 °C and supernatants transferred to a new tube.

Proteins from conditioned medium and cell lysates were separated by SDS-PAGE under reducing conditions in Tris/Glycine/SDS running buffer for 35 min at 200 V and transferred onto PVDF membranes (Bio-Rad Laboratories) in Tris/Glycine buffer with 20% methanol for 53 min at 100 V at 4 °C. Membranes were blocked with 1% Casein in PBS (Thermo Fisher Scientific) for 1h at RT and incubated overnight with rabbit anti-DYKDDDDK (FLAG) Tag antibody (Cat. # 14793S, Cell Signaling Technology) diluted 1:500 in blocking buffer with 0.1% Tween-20 (PBST). Membranes were washed three times for 5 min with PBST and incubated with IRDye 800CW donkey-anti-rabbit secondary antibody (LI-COR) diluted 1: 1000 in blocking buffer with 0.1% Tween-20 and 0.02% SDS for 40 min at RT. Membranes were washed three times for 5 min with PBST, once with PBS for 5 min at RT, and scanned on a ChemiDoc MP Imaging System (Bio-Rad).

Immunocytochemistry

HEK293T cells transfected with wt and G661R mutant forms of human ADAMTS10 were seeded in 4-well chamber slides (Cat.# 154526, Lab-Tek, Thermo Fisher Scientific) and cultured in DMEM supplemented with 10% FBS at 37 °C in a humidified incubator with a 5% CO_2 atmosphere for 3 days. Cells were rinsed once with PBS and fixed with freshly made 4% PFA in PBS for 15 min. After rinsing with PBS, cells were blocked with 2% bovine serum albumin (BSA) (Jackson Immuno Research Laboratories) in PBS for 1h at RT, then incubated with rabbit anti-FLAG-Tag primary antibody diluted 1:1,000 in blocking buffer for 2h at RT. Cells were washed three times for 5 min with PBS, permeabilized with 0.1% Triton X-100 for 10 min, washed with PBS for 5 min, and incubated with donkey anti-rabbit secondary antibody conjugated with Alexa Fluor 488 fluorophore (Thermo Fisher Scientific) diluted in blocking buffer (1:1,000) and 2.5 μg/ml DAPI (Sigma) for 1h at RT. Cells were washed three times for 5 min with PBS and mounted with ProLong Gold Antifade Mountant (Invitrogen) and imaged using Olympus confocal microscopy equipped with 100X oil immersion objective.

Scotopic flash electroretinogram

Scotopic flash ERG was performed using Espion system equipped with a Ganzfeld dome (ColorDome, Diagnosys). Mice were dark-adapted overnight and anesthetized with ketamine/xylazine/urethane (28/11.2/560 mg/kg). Their pupils were dilated with 1% tropicamide (Bausch & Lomb) and 2.5% phenylephrine (Paragon Biotech). Gold electrodes were placed on the corneas, reference electrodes inserted subcutaneously at the snort and ground electrodes placed subcutaneously at the tail base. ERGs were elicited with white flashes of 4 ms duration, ranging in intensity from −4 to 0 log cd·s/m^2 with 1 log increments. Recordings included a 100 ms pre-stimulus baseline with data collected up to 500 ms after stimuli onset. pSTR and a-wave amplitudes were determined by the peak or trough to baseline. The b-wave amplitudes were calculated from the a-wave trough to the b-wave peak. Latencies were determined as the time intervals from stimulus onset to peak/

trough. Mice at 3–5 months of age were used and results from each eye were considered independently.

Optic nerve analysis

After mice were sacrificed and cardiac perfusion fixed as described above, eyes were enucleated, their optic nerves cut at the chiasm and fixed in 1% glutaraldehyde/4% PFA in PBS. Optic nerves were post-fixed in 2% osmium for 1 h, then dehydrated and embedded in epoxy resin, as previously described.[39] The length of the optic nerve stump attached to the eye was measured by digital caliper. To normalize the distance from the eye from which the optic nerve sections were taken, the block of the nerve was cut in such that the stump length plus the cut in distance along the optic nerve was 1.5 mm for all nerves. Cross sections of the optic nerve of 1 μm thickness were cut using an ultramicrotome (Leica EM UC7, Wetzlar, Germany) and stained with PPD. Images were acquired using an upright light microscope equipped with a 100× 1.45 NA oil immersion objective and SLR camera (DS-Ri2, Nikon, Japan). Tiling images of the whole nerve were assembled in NIS-element software and analyzed in ImageJ (https://imagej.net). A total of 24 boxes drawn in Photoshop were place over the central, medial and peripheral regions of the nerve, covering ~10% of each nerve area.[39] Axons in each box were manually counted and axon density calculated as axon counts divided by box area. Significant decreasing axon density from central to peripheral regions was seen in both wt and $Adamts10^{G661R/G661R}$ mice (data not shown), and therefore axon counts in each region were calculated as the average regional density multiplied by the regional area. Total axon counts were determined by the sum of counts from the three regions. Optic nerve area was measured using the polygon drawing function of ImageJ.

TUNEL assay

Apoptotic cells of the central sagittal retinal sections from postnatal day 10 (P10) mice were detected by terminal deoxynucleotidyl transferase mediated dUTP nick-end labelling (TUNEL, Cat. # G3250, Promega, USA) following manufacturer's instructions. Images were acquired using an upright fluorescence microscope (Nikon, Japan) equipped with a 10× 0.45 NA objective and CMOS camera (Hamamatsu ORCA-Flash 4.0, Japan). TUNEL positive apoptotic cells on the GCL layer were counted from 2 – 5 sections and the mean number of apoptotic cells/section for each retina was reported.

Proximity Ligation Assay

Duolink proximity ligation assay [62] (PLA, DUO92105, Sigma) was performed following the manufacturer's instructions. Briefly, HEK293T cells were transfected with human TGFβ1 and FLAG-tagged ADAMTS10 plasmids in 4-well chamber slides. After 48h, cells were fixed in 4% PFA and permeabilized using 0.1% TritonX-100. Cells were incubated with primary antibodies (anti-LAP-TGF-β1, 1:20, cat. # AF-246-NA; anti-FLAG, 1:1,000, cat. # 14793S, Cell Signaling Biotechnology) for 2h at RT followed by ligation and amplification. Slides were washed and mounted with DAPI-containing mounting medium. Images were acquired using Olympus confocal microscope FV1000 equipped with 60X oil-immersion objective.

Statistical Analysis

Approximately equal numbers of male and female mice were used. Experiments were conducted in a masked fashion. Statistical analysis was performed using GraphPad Prism. A normality test was applied to each data set to determine whether to use t-test for normally distributed data, or otherwise to use Mann-Whitney test as indicated in the figure legends. Data were presented as mean ± SD.

Supplementary Material

Refer to Web version on PubMed Central for supplementary material.

Acknowledgements:

The authors thank Lynn Sakai, PhD (Oregon Health and Science University, Portland, OR, USA) for kindly providing the anti-fibrillin-1 antibody pAb 9543 for this study. We also thank Abudi Nashabi for optic nerve histology and Samyukta Reddy for mouse colony management and genotyping.

This work was supported by NEI grants EY027746 (JK), Vanderbilt Vision Research Center (P30EY008126) and Departmental Unrestricted Award from Research to Prevent Blindness, Inc. Imaging was performed through the Vanderbilt Cell Imaging Shared Resource, which is supported by grants from the National Institutes of Health (CA68485, DK20593, DK58404, DK59637, and S10 RR023901).

Abbreviations:

ADAMTS	a disintegrin-like and metalloproteinase with thrombospondin type 1 motifs
AH	aqueous humor
BMP	bone morphogenic protein
ECM	extracellular matrix
ERG	electroretinogram
GFAP	glial fibrillary acidic protein
LAP	latency associated protein
LTBP	latent transforming growth factor β binding protein
MAGP1	microfibril-associated glycoprotein 1
MFS	Marfan syndrome
PLA	proximity ligation assay
pSTR	positive scotopic threshold response
RGCs	retinal ganglion cells
TGFβ	transforming growth factor β
WMS	Weill-Marchesani syndrome

References

[1]. Davis BM, Crawley L, Pahlitzsch M, Javaid F, Cordeiro MF, Glaucoma: the retina and beyond, Acta Neuropathol. (Berl.) 132 (2016) 807–826. 10.1007/s00401-016-1609-2. [PubMed: 27544758]

[2]. Calkins DJ, Critical pathogenic events underlying progression of neurodegeneration in glaucoma, Prog. Retin. Eye Res 31 (2012) 702–719. 10.1016/j.preteyeres.2012.07.001. [PubMed: 22871543]

[3]. Kuchtey J, Olson LM, Rinkoski T, MacKay EO, Iverson TM, Gelatt KN, Haines JL, Kuchtey RW, Mapping of the Disease Locus and Identification of ADAMTS10 As a Candidate Gene in a Canine Model of Primary Open Angle Glaucoma, PLOS Genet. 7 (2011) e1001306. 10.1371/journal.pgen.1001306. [PubMed: 21379321]

[4]. Apte SS, A Disintegrin-like and Metalloprotease (Reprolysin-type) with Thrombospondin Type 1 Motif (ADAMTS) Superfamily: Functions and Mechanisms*, J. Biol. Chem 284 (2009) 31493–31497. 10.1074/jbc.R109.052340. [PubMed: 19734141]

[5]. Ahonen SJ, Kaukonen M, Nussdorfer FD, Harman CD, Komáromy AM, Lohi H, A Novel Missense Mutation in ADAMTS10 in Norwegian Elkhound Primary Glaucoma, PLOS ONE. 9 (2014) e111941. 10.1371/journal.pone.0111941. [PubMed: 25372548]

[6]. Forman OP, Pettitt L, Komáromy AM, Bedford P, Mellersh C, A Novel Genome-Wide Association Study Approach Using Genotyping by Exome Sequencing Leads to the Identification of a Primary Open Angle Glaucoma Associated Inversion Disrupting ADAMTS17, PLOS ONE. 10 (2015) e0143546. 10.1371/journal.pone.0143546. [PubMed: 26683476]

[7]. Oliver JAC, Forman OP, Pettitt L, Mellersh CS, Two Independent Mutations in ADAMTS17 Are Associated with Primary Open Angle Glaucoma in the Basset Hound and Basset Fauve de Bretagne Breeds of Dog, PLOS ONE. 10 (2015) e0140436. 10.1371/journal.pone.0140436. [PubMed: 26474315]

[8]. Oliver JAC, Rustidge S, Pettitt L, Jenkins CA, Farias FHG, Giuliano EA, Mellersh CS, Evaluation of ADAMTS17 in Chinese Shar-Pei with primary open-angle glaucoma, primary lens luxation, or both, Am. J. Vet. Res 79 (2018) 98–106. 10.2460/ajvr.79.1.98. [PubMed: 29287154]

[9]. Springelkamp H, Höhn R, Mishra A, Hysi PG, Khor C-C, Loomis SJ, Bailey JNC, Gibson J, Thorleifsson G, Janssen SF, Luo X, Ramdas WD, Vithana E, Nongpiur ME, Montgomery GW, Xu L, Mountain JE, Gharahkhani P, Lu Y, Amin N, Karssen LC, Sim K-S, van Leeuwen EM, Iglesias AI, Verhoeven VJM, Hauser MA, Loon S-C, Despriet DDG, Nag A, Venturini C, Sanfilippo PG, Schillert A, Kang JH, Landers J, Jonasson F, Cree AJ, van Koolwijk LME, Rivadeneira F, Souzeau E, Jonsson V, Menon G, Blue Mountains Eye Study—GWAS group, Weinreb RN, de Jong PTVM, Oostra BA, Uitterlinden AG, Hofman A, Ennis S, Thorsteinsdottir U, Burdon KP, NEIGHBORHOOD Consortium, Wellcome Trust Case Control Consortium 2 (WTCCC2), Spector TD, Mirshahi A, Saw S-M, Vingerling JR, Teo Y-Y, Haines JL, Wolfs RCW, Lemij HG, Tai E-S, Jansonius NM, Jonas JB, Cheng C-Y, Aung T, Viswanathan AC, Klaver CCW, Craig JE, Macgregor S, Mackey DA, Lotery AJ, Stefansson K, Bergen AAB, Young TL, Wiggs JL, Pfeiffer N, Wong T-Y, Pasquale LR, Hewitt AW, van Duijn CM, Hammond CJ, Meta-analysis of genome-wide association studies identifies novel loci that influence cupping and the glaucomatous process, Nat. Commun 5 (2014) 4883. 10.1038/ncomms5883. [PubMed: 25241763]

[10]. Springelkamp H, Mishra A, Hysi PG, Gharahkhani P, Höhn R, Khor C-C, Cooke Bailey JN, Luo X, Ramdas WD, Vithana E, Koh V, Yazar S, Xu L, Forward H, Kearns LS, Amin N, Iglesias AI, Sim K-S, van Leeuwen EM, Demirkan A, van der Lee S, Loon S-C, Rivadeneira F, Nag A, Sanfilippo PG, Schillert A, de Jong PTVM, Oostra BA, Uitterlinden AG, Hofman A, Zhou T, Burdon KP, Spector TD, Lackner KJ, Saw S-M, Vingerling JR, Teo Y-Y, Pasquale LR, Wolfs RCW, Lemij HG, Tai E-S, Jonas JB, Cheng C-Y, Aung T, Jansonius NM, Klaver CCW, Craig JE, Young TL, Haines JL, MacGregor S, Mackey DA, Pfeiffer N, Wong T-Y, Wiggs JL, Hewitt AW, van Duijn CM, Hammond CJ, Meta-analysis of Genome-Wide Association Studies Identifies Novel Loci Associated With Optic Disc Morphology, Genet. Epidemiol 39 (2015) 207–216. 10.1002/gepi.21886. [PubMed: 25631615]

[11]. Springelkamp H, Iglesias AI, Mishra A, Höhn R, Wojciechowski R, Khawaja AP, Nag A, Wang YX, Wang JJ, Cuellar-Partida G, Gibson J, Bailey JNC, Vithana EN, Gharahkhani P, Boutin T, Ramdas WD, Zeller T, Luben RN, Yonova-Doing E, Viswanathan AC, Yazar S, Cree AJ, Haines JL, Koh JY, Souzeau E, Wilson JF, Amin N, Müller C, Venturini C, Kearns LS, Kang JH, Tham YC, Zhou T, Leeuwen V, Nickels EM,S, Sanfilippo P, Liao J, van der Linde H, Zhao W, Koolwijk V, M.e L, Zheng L, Rivadeneira F, Baskaran M, Lee VD, Perera SJ,S, Jong D, T.v.m P, Oostra BA, Uitterlinden AG, Fan Q, Hofman A, Tai E-S, Vingerling JR, Sim X, Wolfs RCW, Teo YY, Lemij HG, Khor CC, Willemsen R, Lackner KJ, Aung T, Jansonius NM, Montgomery G, Wild PS, Young TL, Burdon KP, Hysi PG, Pasquale LR, Wong TY, Klaver CCW, Hewitt AW, Jonas JB, Mitchell P, Lotery AJ, Foster PJ, Vitart V, Pfeiffer N, Craig JE, Mackey DA, Hammond CJ, Wiggs JL, Cheng C-Y, Duijn V, C. M, S. MacGregor, New insights into the genetics of primary open-angle glaucoma based on meta-analyses of intraocular pressure and optic disc characteristics, Hum. Mol. Genet 26 (2017) 438–453. 10.1093/hmg/ddw399. [PubMed: 28073927]

[12]. Iglesias AI, Mishra A, Vitart V, Bykhovskaya Y, Höhn R, Springelkamp H, Cuellar-Partida G, Gharahkhani P, Bailey JNC, Willoughby CE, Li X, Yazar S, Nag A, Khawaja AP, Polašek O, Siscovick D, Mitchell P, Tham YC, Haines JL, Kearns LS, Hayward C, Shi Y, van Leeuwen EM, Taylor KD, Blue Mountains Eye Study—GWAS group, Bonnemaijer P, Rotter JI, Martin NG, Zeller T, Mills RA, Souzeau E, Staffieri SE, Jonas JB, Schmidtmann I, Boutin T, Kang JH, Lucas SEM, Wong TY, Beutel ME, Wilson JF, NEIGHBORHOOD Consortium, Wellcome Trust Case Control Consortium 2 (WTCCC2), Uitterlinden AG, Vithana EN, Foster PJ, Hysi PG, Hewitt AW, Khor CC, Pasquale LR, Montgomery GW, Klaver CCW, Aung T, Pfeiffer N, Mackey DA, Hammond CJ, Cheng C-Y, Craig JE, Rabinowitz YS, Wiggs JL, Burdon KP, van Duijn CM, MacGregor S, Cross-ancestry genome-wide association analysis of corneal thickness strengthens link between complex and Mendelian eye diseases, Nat. Commun 9 (2018) 1864. 10.1038/s41467-018-03646-6. [PubMed: 29760442]

[13]. Hendee K, Wang LW, Reis LM, Rice GM, Apte SS, Semina EV, Identification and functional analysis of an ADAMTSL1 variant associated with a complex phenotype including congenital glaucoma, craniofacial, and other systemic features in a three-generation human pedigree, Hum. Mutat 38 (2017) 1485–1490. 10.1002/humu.23299. [PubMed: 28722276]

[14]. Dagoneau N, Benoist-Lasselin C, Huber C, Faivre L, Mégarbané A, Alswaid A, Dollfus H, Alembik Y, Munnich A, Legeai-Mallet L, Cormier-Daire V, ADAMTS10 Mutations in Autosomal Recessive Weill-Marchesani Syndrome, Am. J. Hum. Genet 75 (2004) 801–806. 10.1086/425231. [PubMed: 15368195]

[15]. Morales J, Al-Sharif L, Khalil DS, Shinwari JMA, Bavi P, Al-Mahrouqi RA, Al-Rajhi A, Alkuraya FS, Meyer BF, Al Tassan N, Homozygous Mutations in ADAMTS10 and ADAMTS17 Cause Lenticular Myopia, Ectopia Lentis, Glaucoma, Spherophakia, and Short Stature, Am. J. Hum. Genet 85 (2009) 558–568. 10.1016/j.ajhg.2009.09.011. [PubMed: 19836009]

[16]. Kutz WE, Wang LW, Dagoneau N, Odrcic KJ, Cormier-Daire V, Traboulsi EI, Apte SS, Functional analysis of an ADAMTS10 signal peptide mutation in Weill-Marchesani syndrome demonstrates a long-range effect on secretion of the full-length enzyme, Hum. Mutat 29 (2008) 1425–1434. 10.1002/humu.20797. [PubMed: 18567016]

[17]. Faivre L, Gorlin RJ, Wirtz MK, Godfrey M, Dagoneau N, Samples JR, Merrer ML, Collod-Beroud G, Boileau C, Munnich A, Cormier-Daire V, In frame fibrillin-1 gene deletion in autosomal dominant Weill-Marchesani syndrome, J. Med. Genet 40 (2003) 34–36. 10.1136/jmg.40.1.34. [PubMed: 12525539]

[18]. Sengle G, Tsutsui K, Keene DR, Tufa SF, Carlson EJ, Charbonneau NL, Ono RN, Sasaki T, Wirtz MK, Samples JR, Fessler LI, Fessler JH, Sekiguchi K, Hayflick SJ, Sakai LY, Microenvironmental Regulation by Fibrillin-1, PLOS Genet. 8 (2012) e1002425. 10.1371/journal.pgen.1002425. [PubMed: 22242013]

[19]. Faivre L, Dollfus H, Lyonnet S, Alembik Y, Mégarbané A, Samples J, Gorlin RJ, Alswaid A, Feingold J, Merrer ML, Munnich A, Cormier-Daire V, Clinical homogeneity and genetic heterogeneity in Weill–Marchesani syndrome, Am. J. Med. Genet. A 123A (2003) 204–207. 10.1002/ajmg.a.20289. [PubMed: 14598350]

[20]. Hubmacher D, Apte SS, Genetic and functional linkage between ADAMTS superfamily proteins and fibrillin-1: a novel mechanism influencing microfibril assembly and function, Cell. Mol. Life Sci 68 (2011) 3137. 10.1007/s00018-011-0780-9. [PubMed: 21858451]

[21]. Kutz WE, Wang LW, Bader HL, Majors AK, Iwata K, Traboulsi EI, Sakai LY, Keene DR, Apte SS, ADAMTS10 Protein Interacts with Fibrillin-1 and Promotes Its Deposition in Extracellular Matrix of Cultured Fibroblasts, J. Biol. Chem 286 (2011) 17156–17167. 10.1074/jbc.M111.231571. [PubMed: 21402694]

[22]. Mularczyk EJ, Singh M, Godwin ARF, Galli F, Humphreys N, Adamson AD, Mironov A, Cain SA, Sengle G, Boot-Handford RP, Cossu G, Kielty CM, Baldock C, ADAMTS10-mediated tissue disruption in Weill–Marchesani syndrome, Hum. Mol. Genet. (n.d.) 10.1093/hmg/ddy276.

[23]. Wu H-J, Mortlock DP, Kuchtey RW, Kuchtey J, Altered Ocular Fibrillin Microfibril Composition in Mice With a Glaucoma-Causing Mutation of Adamts10, Invest. Ophthalmol. Vis. Sci 62 (2021) 26–26. 10.1167/iovs.62.10.26.

[24]. Wang LW, Kutz WE, Mead TJ, Beene LC, Singh S, Jenkins MW, Reinhardt DP, Apte SS, Adamts10 inactivation in mice leads to persistence of ocular microfibrils subsequent to reduced fibrillin-2 cleavage, Matrix Biol. (2018). 10.1016/j.matbio.2018.09.004.

[25]. Dietz HC, Cutting GR, et al. , Marfan Syndrome Caused by a Recurrent de novo Missense Mutation in the Fibrillin Gene, Nature. 352 (1991) 337–9. [PubMed: 1852208]

[26]. Comeglio P, Evans AL, Brice G, Cooling RJ, Child AH, Identification of FBN1 gene mutations in patients with ectopia lentis and marfanoid habitus, Br. J. Ophthalmol 86 (2002) 1359–1362. [PubMed: 12446365]

[27]. Sakai LY, Keene DR, Renard M, De Backer J, FBN1: The disease-causing gene for Marfan syndrome and other genetic disorders, Gene. 591 (2016) 279–291. 10.1016/j.gene.2016.07.033. [PubMed: 27437668]

[28]. Ramirez F, Rifkin DB, Extracellular microfibrils: contextual platforms for TGFβ and BMP signaling, Curr. Opin. Cell Biol 21 (2009) 616–622. 10.1016/j.ceb.2009.05.005. [PubMed: 19525102]

[29]. Tzavlaki K, Moustakas A, TGF-β Signaling, Biomolecules. 10 (2020) 487. 10.3390/biom10030487. [PubMed: 32210029]

[30]. Neptune ER, Frischmeyer PA, Arking DE, Myers L, Bunton TE, Gayraud B, Ramirez F, Sakai LY, Dietz HC, Dysregulation of TGF-β activation contributes to pathogenesis in Marfan syndrome, Nat. Genet 33 (2003) 407–411. 10.1038/ng1116. [PubMed: 12598898]

[31]. Habashi JP, Judge DP, Holm TM, Cohn RD, Loeys BL, Cooper TK, Myers L, Klein EC, Liu G, Calvi C, Podowski M, Neptune ER, Halushka MK, Bedja D, Gabrielson K, Rifkin DB, Carta L, Ramirez F, Huso DL, Dietz HC, Losartan, an AT1 Antagonist, Prevents Aortic Aneurysm in a Mouse Model of Marfan Syndrome, Science. 312 (2006) 117–121. 10.1126/science.1124287. [PubMed: 16601194]

[32]. Oichi T, Taniguchi Y, Soma K, Oshima Y, Yano F, Mori Y, Chijimatsu R, Kim-Kaneyama J, Tanaka S, Saito T, Adamts17 is involved in skeletogenesis through modulation of BMP-Smad1/5/8 pathway, Cell. Mol. Life Sci 76 (2019) 4795–4809. 10.1007/s00018-019-03188-0. [PubMed: 31201465]

[33]. Fuchshofer R, Tamm ER, The role of TGF-β in the pathogenesis of primary open-angle glaucoma, Cell Tissue Res. 347 (2012) 279–290. 10.1007/s00441-011-1274-7. [PubMed: 22101332]

[34]. Mecham RP, Gibson MA, The microfibril-associated glycoproteins (MAGPs) and the microfibrillar niche, Matrix Biol. 47 (2015) 13–33. 10.1016/j.matbio.2015.05.003. [PubMed: 25963142]

[35]. Saszik SM, Robson JG, Frishman LJ, The scotopic threshold response of the dark-adapted electroretinogram of the mouse, J. Physiol 543 (2002) 899–916. 10.1113/jphysiol.2002.019703. [PubMed: 12231647]

[36]. Bui BV, Fortune B, Ganglion cell contributions to the rat full-field electroretinogram, J. Physiol 555 (2004) 153–173. 10.1113/jphysiol.2003.052738. [PubMed: 14578484]

[37]. Alarcón-Martínez L, Avilés-Trigueros M, Galindo-Romero C, Valiente-Soriano J, Agudo-Barriuso M, de la Villa P, Villegas-Pérez MP, Vidal-Sanz M, ERG changes in albino and

pigmented mice after optic nerve transection, Vision Res. 50 (2010) 2176–2187. 10.1016/j.visres.2010.08.014. [PubMed: 20727908]

[38]. Liu Y, McDowell CM, Zhang Z, Tebow HE, Wordinger RJ, Clark AF, Monitoring Retinal Morphologic and Functional Changes in Mice Following Optic Nerve Crush, Invest. Ophthalmol. Vis. Sci 55 (2014) 3766–3774. 10.1167/iovs.14-13895. [PubMed: 24854856]

[39]. Wu H-J, Hazlewood RJ, Kuchtey J, Kuchtey RW, Enlarged Optic Nerve Axons and Reduced Visual Function in Mice with Defective Microfibrils, ENeuro. 5 (2018). 10.1523/ENEURO.0260-18.2018.

[40]. Zhu Y, Pappas AC, Wang R, Seifert P, Sun D, Jakobs TC, Ultrastructural Morphology of the Optic Nerve Head in Aged and Glaucomatous Mice, Invest. Ophthalmol. Vis. Sci 59 (2018) 3984–3996. 10.1167/iovs.18-23885. [PubMed: 30098187]

[41]. Cooper ML, Crish SD, Inman DM, Horner PJ, Calkins DJ, Early astrocyte redistribution in the optic nerve precedes axonopathy in the DBA/2J mouse model of glaucoma, Exp. Eye Res. (n.d.) 10.1016/j.exer.2015.11.016.

[42]. Braunger BM, Demmer C, Tamm ER, Programmed Cell Death During Retinal Development of the Mouse Eye, in: Ash JD, Grimm C, Hollyfield JG, Anderson RE, LaVail MM, Bowes Rickman C (Eds.), Retin. Degener. Dis, Springer, New York, NY, 2014: pp. 9–13. 10.1007/978-1-4614-3209-8_2.

[43]. Bourd-Boittin K, Bonnier D, Leyme A, Mari B, Tuffery P, Samson M, Ezan F, Baffet G, Theret N, Protease profiling of liver fibrosis reveals the ADAM metallopeptidase with thrombospondin type 1 motif, 1 as a central activator of transforming growth factor beta, Hepatology. 54 (2011) 2173–2184. 10.1002/hep.24598. [PubMed: 21826695]

[44]. Yao Y, Hu C, Song Q, Li Y, Da X, Yu Y, Li H, Clark IM, Chen Q, Wang QK, ADAMTS16 activates latent TGF-β, accentuating fibrosis and dysfunction of the pressure-overloaded heart, Cardiovasc. Res 116 (2020) 956–969. 10.1093/cvr/cvz187. [PubMed: 31297506]

[45]. Somerville RPT, Jungers KA, Apte SS, Discovery and Characterization of a Novel, Widely Expressed Metalloprotease, ADAMTS10, and Its Proteolytic Activation, J. Biol. Chem 279 (2004) 51208–51217. 10.1074/jbc.M409036200. [PubMed: 15355968]

[46]. Karoulias SZ, Beyens A, Balic Z, Symoens S, Vandersteen A, Rideout AL, Dickinson J, Callewaert B, Hubmacher D, A novel ADAMTS17 variant that causes Weill-Marchesani syndrome 4 alters fibrillin-1 and collagen type I deposition in the extracellular matrix, Matrix Biol. (2019). 10.1016/j.matbio.2019.11.001.

[47]. Baldwin AK, Simpson A, Steer R, Cain SA, Kielty CM, Elastic fibres in health and disease, Expert Rev. Mol. Med 15 (2013). 10.1017/erm.2013.9.

[48]. Wu H-J, Kuchtey J, Kuchtey RW, Increased Susceptibility to Glaucomatous Damage in Microfibril Deficient Mice, Invest. Ophthalmol. Vis. Sci 61 (2020) 28–28. 10.1167/iovs.61.10.28.

[49]. Jones W, Rodriguez J, Bassnett S, Targeted deletion of fibrillin-1 in the mouse eye results in ectopia lentis and other ocular phenotypes associated with Marfan syndrome, Dis. Model. Mech 12 (2019). 10.1242/dmm.037283.

[50]. Gehle P, Goergen B, Pilger D, Ruokonen P, Robinson PN, Salchow DJ, Biometric and structural ocular manifestations of Marfan syndrome, PLOS ONE. 12 (2017) e0183370. 10.1371/journal.pone.0183370. [PubMed: 28931008]

[51]. Razeghinejad MR, Hosseini H, Namazi N, Biometric and corneal topographic characteristics in patients with Weill-Marchesani syndrome, J. Cataract Refract. Surg 35 (2009) 1026–1032. 10.1016/j.jcrs.2009.01.029. [PubMed: 19465288]

[52]. Braunger BM, Pielmeier S, Demmer C, Landstorfer V, Kawall D, Abramov N, Leibinger M, Kleiter I, Fischer D, Jägle H, Tamm ER, TGF-β Signaling Protects Retinal Neurons from Programmed Cell Death during the Development of the Mammalian Eye, J. Neurosci 33 (2013) 14246–14258. 10.1523/JNEUROSCI.0991-13.2013. [PubMed: 23986258]

[53]. Wareham LK, Whitener AE, Wu H-J, Wu S-Y, Mchaourab HS, Mortlock DP, Kuchtey RW, Kuchtey J, Adamts10 controls transforming growth factor β family signaling that contributes to retinal ganglion cell development, Front. Mol. Biosci 9 (2022). https://www.frontiersin.org/articles/10.3389/fmolb.2022.989851 (accessed September 12, 2022).

[54]. Horiguchi M, Ota M, Rifkin DB, Matrix control of transforming growth factor-β function, J. Biochem. (Tokyo) 152 (2012) 321–329. 10.1093/jb/mvs089. [PubMed: 22923731]

[55]. Yu Q, Stamenkovic I, Cell surface-localized matrix metalloproteinase-9 proteolytically activates TGF-β and promotes tumor invasion and angiogenesis, Genes Dev. 14 (2000) 163–176. 10.1101/gad.14.2.163. [PubMed: 10652271]

[56]. Sato Y, Rifkin DB, Inhibition of endothelial cell movement by pericytes and smooth muscle cells: activation of a latent transforming growth factor-beta 1-like molecule by plasmin during co-culture., J. Cell Biol 109 (1989) 309–315. 10.1083/jcb.109.1.309. [PubMed: 2526131]

[57]. Schultz-Cherry S, Murphy-Ullrich J, Thrombospondin causes activation of latent transforming growth factor-beta secreted by endothelial cells by a novel mechanism, J. Cell Biol 122 (1993) 923–932. 10.1083/jcb.122.4.923. [PubMed: 8349738]

[58]. Schultz-Cherry S, Chen H, Mosher DF, Misenheimer TM, Krutzsch HC, Roberts DD, Murphy-Ullrich JE, Regulation of Transforming Growth Factor-β Activation by Discrete Sequences of Thrombospondin 1 (*), J. Biol. Chem 270 (1995) 7304–7310. 10.1074/jbc.270.13.7304. [PubMed: 7706271]

[59]. Murphy-Ullrich JE, Poczatek M, Activation of latent TGF-β by thrombospondin-1: mechanisms and physiology, Cytokine Growth Factor Rev. 11 (2000) 59–69. 10.1016/S1359-6101(99)00029-5. [PubMed: 10708953]

[60]. Charbonneau NL, Dzamba BJ, Ono RN, Keene DR, Corson GM, Reinhardt DP, Sakai LY, Fibrillins Can Co-assemble in Fibrils, but Fibrillin Fibril Composition Displays Cell-specific Differences*, J. Biol. Chem 278 (2003) 2740–2749. 10.1074/jbc.M209201200. [PubMed: 12429739]

[61]. Hazlewood RJ, Chen Q, Clark FK, Kuchtey J, Kuchtey RW, Differential effects of angiotensin II type I receptor blockers on reducing intraocular pressure and TGFβ signaling in the mouse retina, PLOS ONE. 13 (2018) e0201719. 10.1371/journal.pone.0201719. [PubMed: 30092004]

[62]. Alam MS, Proximity Ligation Assay (PLA), Curr. Protoc. Immunol 123 (2018) e58. 10.1002/cpim.58. [PubMed: 30238640]

Highlights

- G661R mutation of *ADAMTS10* causing glaucoma introduced in mice using CRISPR/Cas9
- ADAMTS10 is expressed along optic nerve axons and in retinal ganglion cells
- ADAMTS10 is not colocalized with fibrillin microfibrils in retina and optic nerve
- ADAMTS10 could function independent of fibrillin
- ADAMTS10 regulates transforming growth factor beta signaling in developing retina

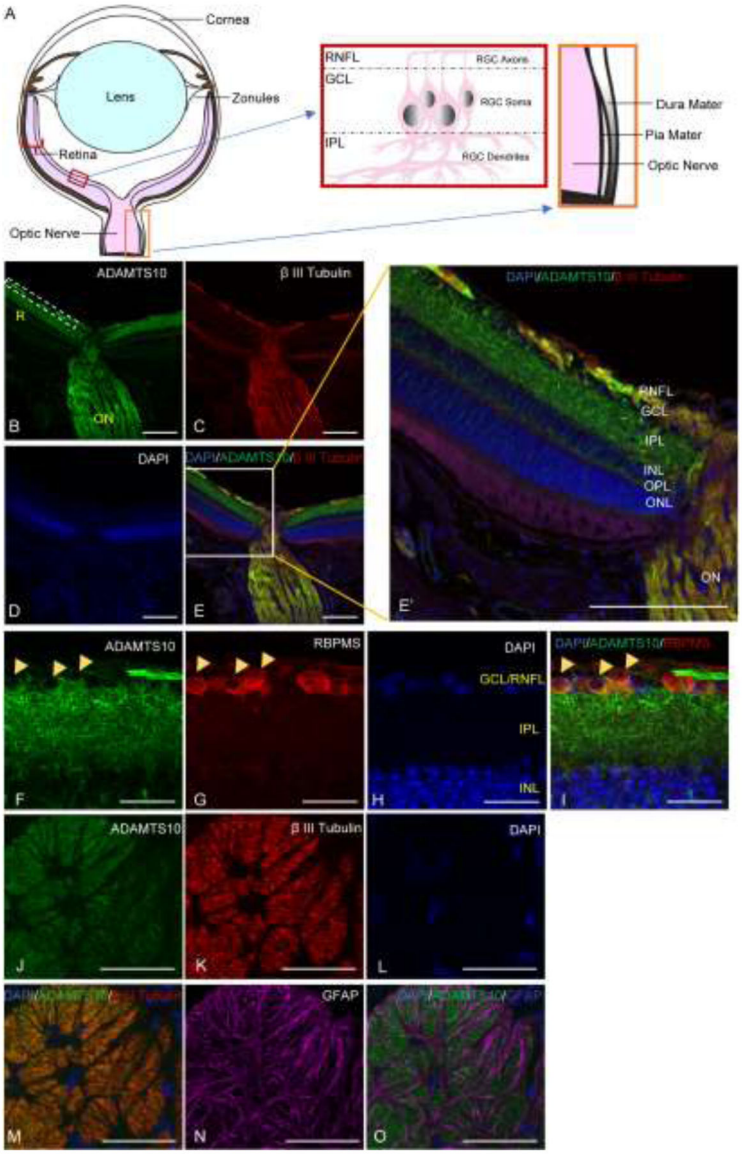

Figure 1. Expression of ADAMTS10 in the retina and optic nerve.

Schematic diagram of the eye (A) showing the cornea, lens, zonules, retina, and optic nerve with zoom in views of the inner retina (red box) and the optic nerve (orange box). RGC axons form the RNFL (red box) and converge at the back of the eye to form the optic nerve which is ensheathed in the pia mater and dura mater (orange box). Immunofluorescent staining of sagittal sections of eyes from mice at 3 months of age showed that ADAMTS10 (green) is primarily expressed in the inner retina and the optic nerve (B). In the retina, the highest intensity of ADAMTS10 immunofluorescence was found in the RNFL (white dashed box, B). Co-staining with a neuronal marker, β III Tubulin (C, red) showed that ADAMTS10 immunofluorescence is highly colocalized with β III Tubulin at the RNFL and the optic nerve axons (E). A zoom in view of the white box in E is shown in E'. Sections were counter-stained with DAPI (D, H and L). High magnification images from co-staining of ADAMTS10 (F, green) with an RGC specific marker, RBPMS (G, red)

showed that ADAMTS10 is associated with RGC soma (yellow arrows, I). In cross-sectional optic nerve sections (J - O), co-staining for ADAMTS10 (J, green), β III Tubulin (K, red) and an astrocyte marker, GFAP (N, purple) revealed that ADAMTS10 immunofluorescence is completely overlapped with β III Tubulin (M) but not with GFAP (O). Scale bar in B - E and E' and J - O: 100 μm. Scale bar in F – I: 20 μm. Blue: DAPI. R: retina; ON: optic nerve; GCL: ganglion cell layer; RNFL: retinal nerve fiber layer; IPL: inner plexiform layer; INL: inner nuclear layer; OPL: outer plexiform layer; ONL: outer nuclear layer.

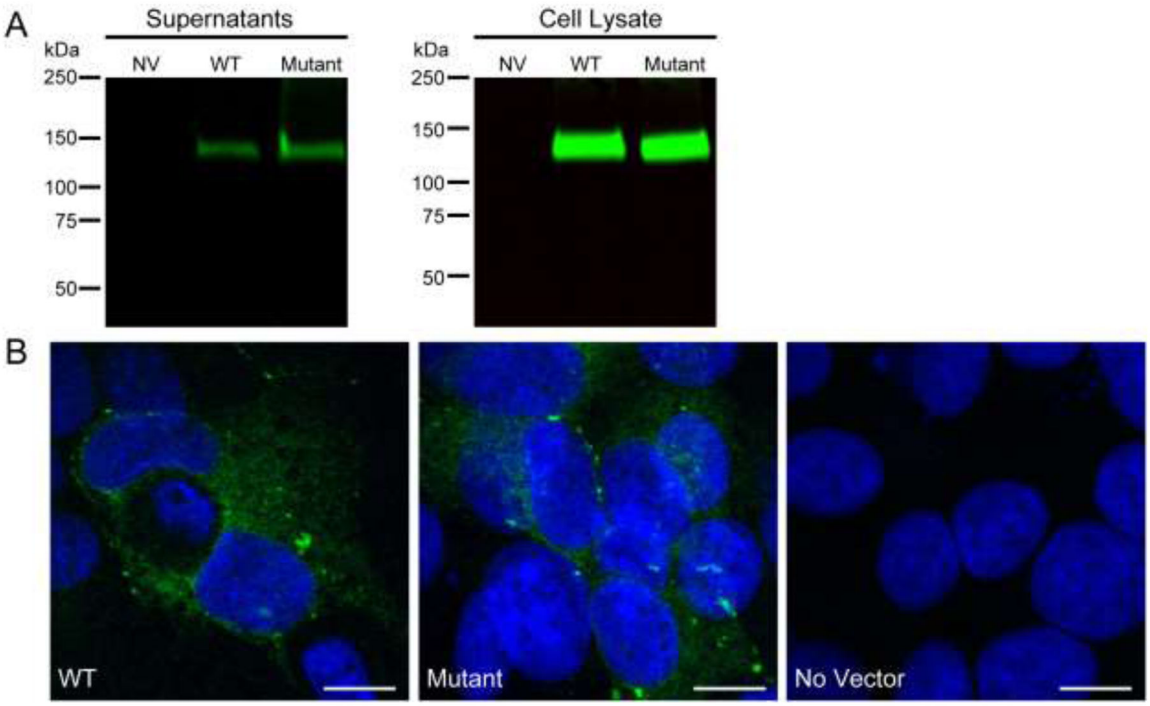

Figure 2. Wild type and mutant forms of human ADAMTS10 are secreted.

HEK293T cells were transfected with either wt or G661R mutant forms of human ADAMTS10. Supernatants and cell lysates were collected for Western blotting under reducing conditions. Bands for FLAG-tagged human ADAMTS10 were detected at the expected molecular weight of ~130 kDa in both supernatants and cell lysates (A). Anti-FLAG immunocytochemistry of non-permeabilized HEK293T cells (B) showed fluorescent signals (green) from cells that were transfected with wt (B, left) and G661R mutant (B, middle) forms of FLAG-tagged human ADAMTS10. No fluorescent signal was detected from cells that were transfected without vectors (B, right). Cell nuclei were counterstained with DAPI (blue). NV: No vector. Scale bar: 10 μm.

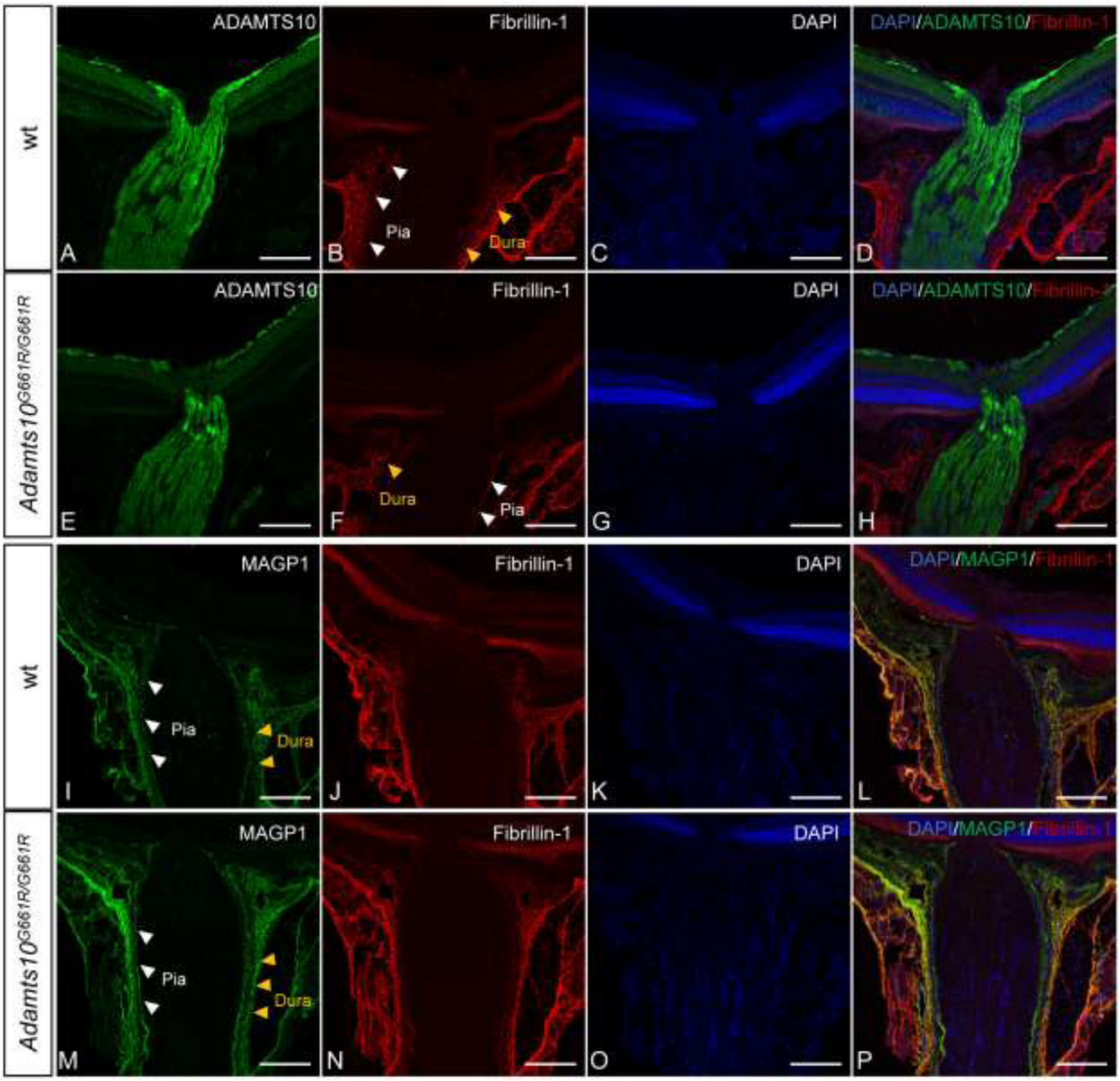

Figure 3. ADAMTS10 is not colocalized with microfibrils in the retina and optic nerve.

In sagittal sections of eyes from wt and *Adamts10*$^{G661R/G661R}$ mice at 3 months of age, double staining for ADAMTS10 (A and E, green) and fibrillin-1 (B and F, red) showed that ADAMTS10 immunofluorescence is expressed in the inner retina and confined to the optic nerve (D and H). Fibrillin-1 immunofluorescence is found in the pia mater (B and F, white arrowheads) and dura mater (B and F, yellow arrowheads) but not in the optic nerve and retina resulting in apparent lack of colocalization of fibrillin-1 and ADAMTS10 (D and H). Co-staining for MAGP1 (I and M, green) and fibrillin-1 (J and N, red) showed that MAGP1 immunofluorescence is colocalized with fibrillin-1 (L and P) in the pia mater and dura mater but is not detected in the optic nerve. The immunofluorescent intensities of ADAMTS10 (A and E), fibrillin-1 (B, J and F, N) and MAGP1 (I and M) were comparable between wt and *Adamts10*$^{G661R/G661R}$ mice. Scale bar: 100 μm. Blue in C, G, K and O: DAPI.

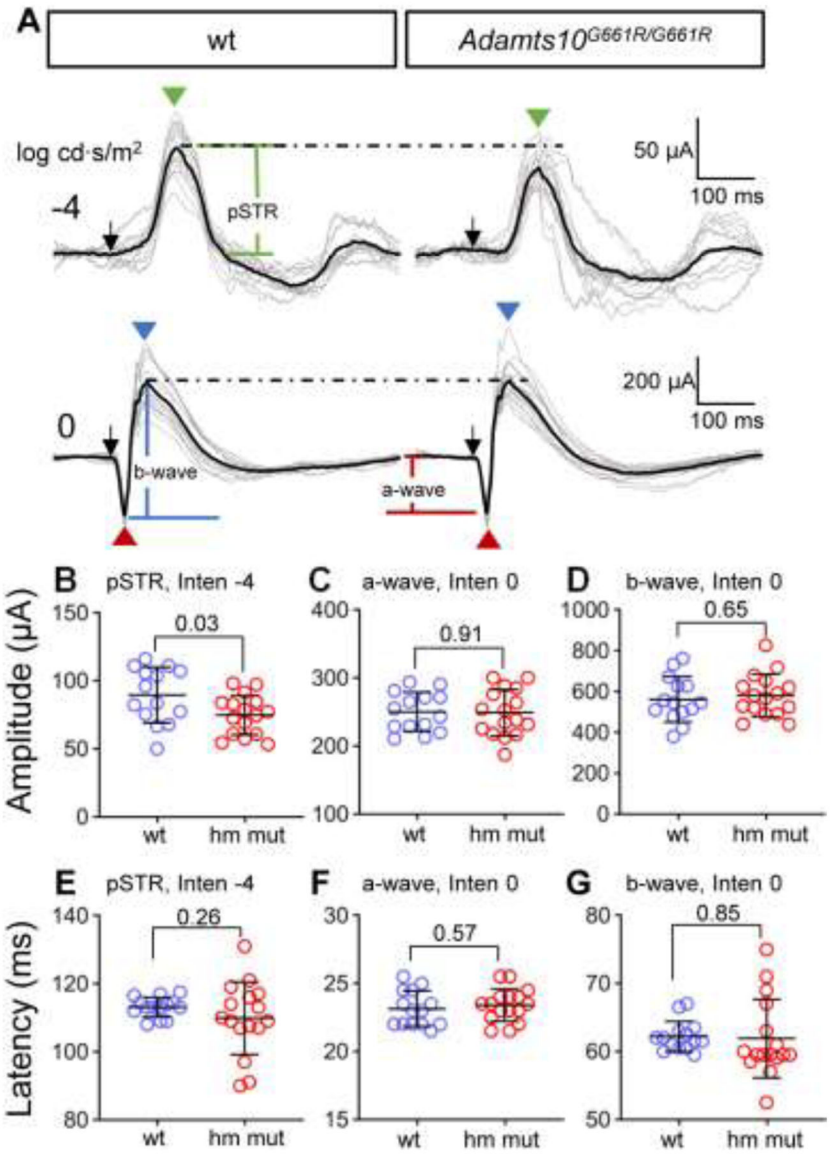

Figure 4. Reduced pSTR amplitude of *Adamts10*$^{G661R/G661R}$ mice at 3–5 months of age.

Scotopic flash ERG waveforms of individual mice (A, gray traces) and average waveforms (A, black traces) in response to stimulus intensities of −4 and 0 log cd·s/m^2 are shown (A). Stimulus onset is indicated by black arrows. Representative temporal locations of the pSTR, a- and b-wave are indicated by green, red and blue arrowheads, respectively. Scales for amplitude and time are indicated on the right side of each row. Left column: wt; right column: *Adamts10*$^{G661R/G661R}$ mice. Amplitude (B – D) and latency (E – G) for pSTR, a- and b-wave were analyzed at stimulus intensities of −4 and 0 log cd·s/m^2, respectively. Significantly reduced pSTR amplitude was found for *Adamts10*$^{G661R/G661R}$ mice, compared to wt (B). Amplitude of a- and b-wave are not significantly different between wt and *Adamts10*$^{G661R/G661R}$ mice (C and D). Latencies of pSTR, a- and b-wave are not significantly different between wt and *Adamts10*$^{G661R/G661R}$ mice (E – G). Stimulus intensities are indicated above each panel. Blue symbols: individual wt mice; red symbols:

individual *Adamts10*$^{G661R/G661R}$ mice. Error bars represent mean ± SD. P values from Student's t-test are indicated above each bracket. hm mut: *Adamts10*$^{G661R/G661R}$ mice. wt: n = 7; *Adamts10*$^{G661R/G661R}$ mice: n = 8. Individual eyes were considered independently.

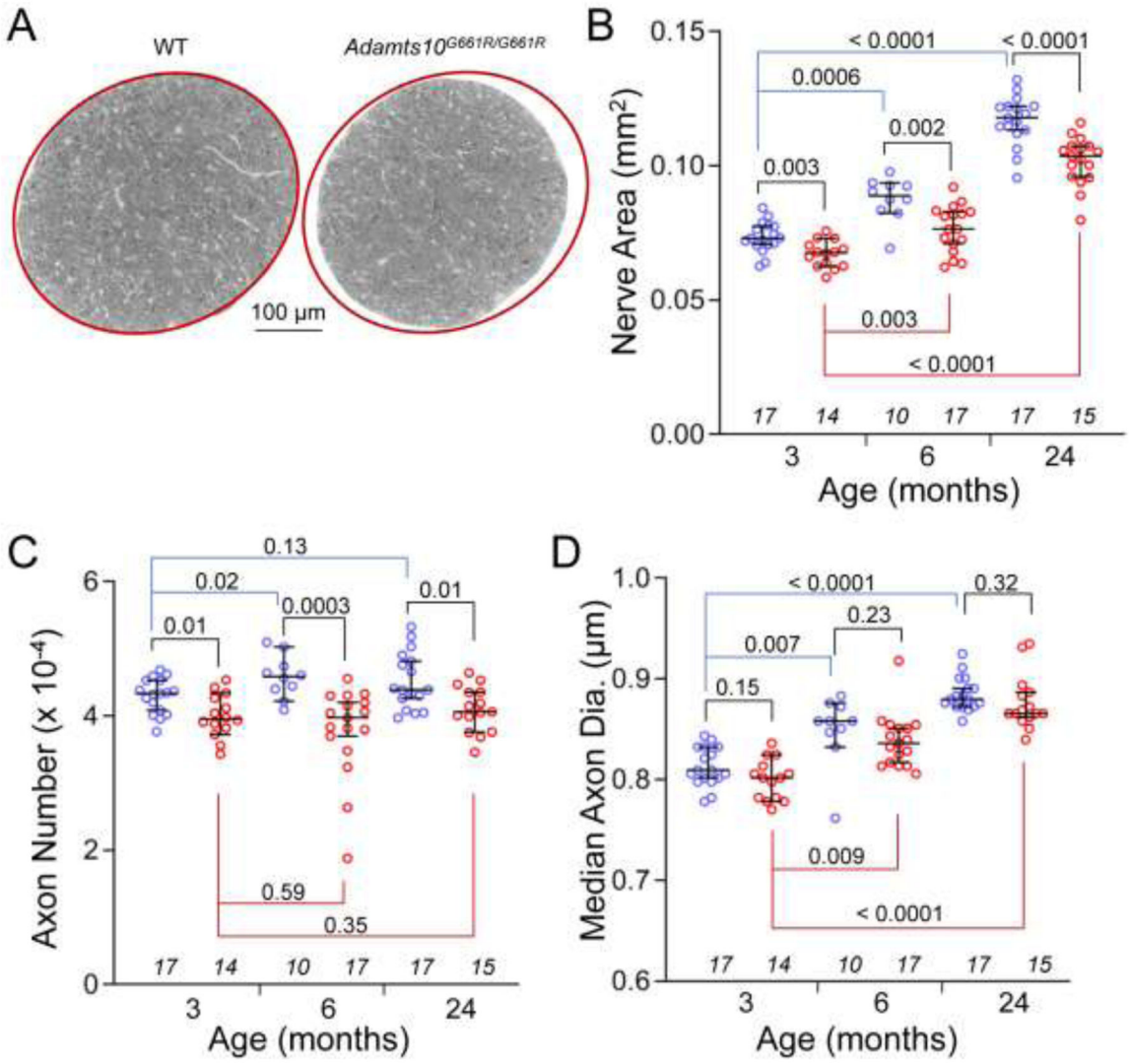

Figure 5. Optic nerve pathology of *Adamts10*$^{G661R/G661R}$ mice.

Adamts10$^{G661R/G661R}$ mice appeared to have smaller optic nerves compared to wt, as shown for representative PPD-stained cross-sectional nerve images of wt (A, left) and *Adamts10*$^{G661R/G661R}$ mice (A, right) at 24 months of age. Optic nerve area was significantly smaller for *Adamts10*$^{G661R/G661R}$ mice at 3, 6 and 24 months of age compared to wt and significantly increased with age for wt and *Adamts10*$^{G661R/G661R}$ mice (B). Reduced optic nerve axon number was found for *Adamts10*$^{G661R/G661R}$ mice compared to wt at 3, 6 and 24 months of age (C). Median axon diameter for *Adamts10*$^{G661R/G661R}$ mice was not significantly different from wt at each time point (D). Median optic nerve axon diameter significantly increased with age for wt and *Adamts10*$^{G661R/G661R}$ mice (D). Blue symbols: individual wt mice; red symbols: individual *Adamts10*$^{G661R/G661R}$ Error bars represent median/95%CI. P values from Mann-Whitney test for B – D are indicated above each bracket. Numbers of mice indicated in italics below each group.

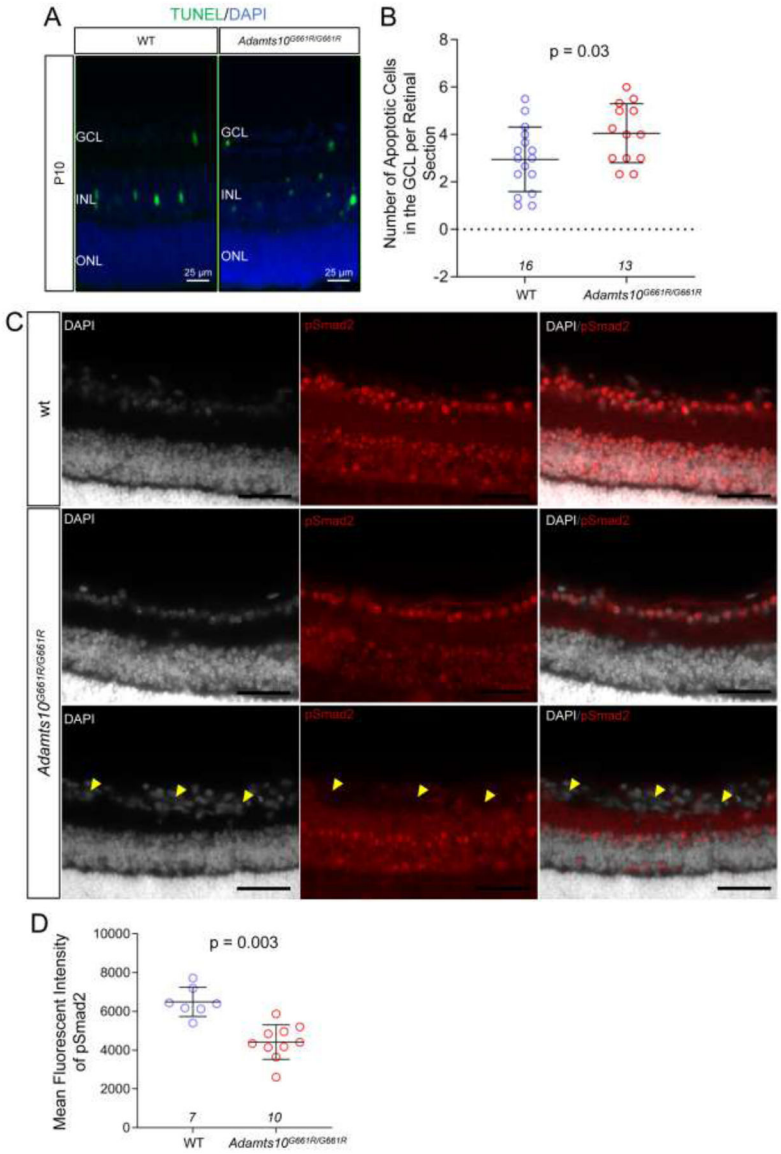

Figure 6. Increased TUNEL-positive apoptotic cells and decreased pSmad2 signals in the GCL of the retina for *Adamts10*$^{G661R/G661R}$ mice at postnatal day 10 (P10).

TUNEL-positive nuclei (green) in P10 retinas of wt and *Adamts10*$^{G661R/G661R}$ mice (A). Quantitative analysis showed significantly higher number of TUNEL-positive apoptotic cells in the GCL for *Adamts10*$^{G661R/G661R}$ mice compared to wt (B). In the GCL of the retina, immunofluorescent intensity of pSmad2 appeared to be lower for *Adamts10*$^{G661R/G661R}$ mice (C, middle row, red) compared to wt (C, top row). In some cases, absence of pSmad2 immunofluorescence (C, yellow arrowheads) with well-preserved nuclei (gray) was found in the retina of *Adamts10*$^{G661R/G661R}$ mice. Mean fluorescence intensity of pSmad2 in the GCL was significantly lower for *Adamts10*$^{G661R/G661R}$ mice compared to wt (D). Error bars represent mean ± SD. P values from Student's t-test are indicated in B and D. Scale bar in C: 50 μM. GCL: ganglion cell layer; INL: inner nuclear layer; ONL: outer nuclear layer. Blue symbols: individual wt mice; red symbols: individual *Adamts10*$^{G661R/G661R}$ mice. Blue in A and gray in C: DAPI. Numbers of mice indicated in italics below each group.

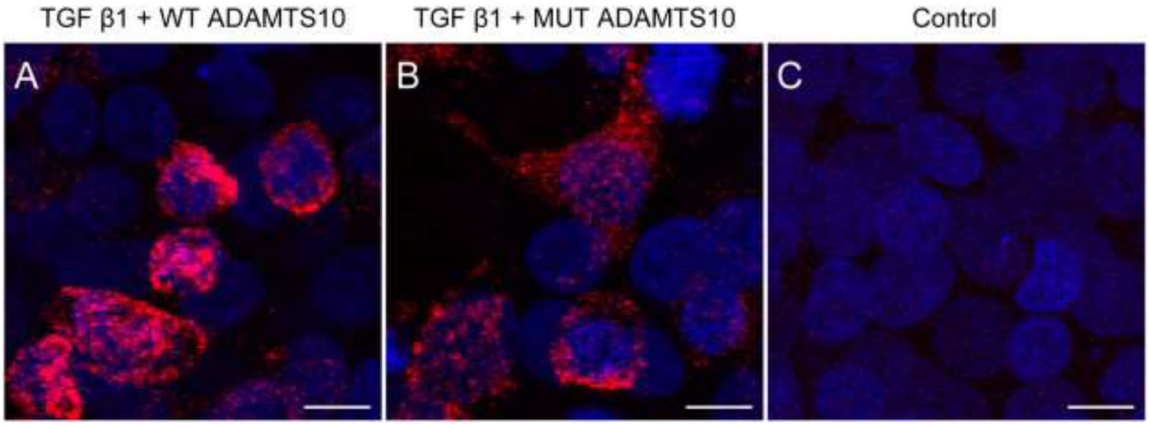

Figure 7. ADAMTS10 and TGFβ1 form interaction complex.

Proximity ligation assays (PLA) to detect protein-protein interactions between LAP-TGFβ and ADAMTS10 were performed on HEK293T cells co-transfected with human TGFβ1 plasmid together with either wt or G661R mutant forms of human FLAG-tagged ADAMTS10. Anti-LAP-TGFβ1 and anti-FLAG antibodies were used to target TGFβ1 and ADAMTS10, respectively. Robust PLA signal indicating interaction (red) was observed in co-transfected cells (A and B). No interaction signal was detected in the control group which omitted primary antibodies (C). Scale bar: 10 μm.

Table 1.

Primary antibodies used for immunofluorescence

Antigen	Host	dilution	Catalog No.	Company
ADAMTS10	goat	1:100	sc-21505	Santa Cruz
RBPMS	rabbit	1:100	GTX118619	GeneTex
Fibrillin-1 * [60]	rabbit	1:200	N/A	N/A
MAGP1	goat	1:100	AF4977	R&D
β III Tubulin	mouse	1:100	903401	Biolegend
GFAP	rabbit	1:1000	Z0334	DAKO
pSmad2	rabbit	1:100	40–0800	Invitrogen

* Polyclonal antibody for fibrillin-1 was kindly provided by Dr. Lynn Sakai.[60]